remote sensing

MDPI

Communication

Prediction of Atmospheric Duct Conditions from a Clutter Power Spectrum Using Deep Learning

Taekyeong Jin, Jeongmin Cho, Doyoung Jang and Hosung Choo *

Department of Electronic and Electrical Engineering, Hongik University, Seoul 04066, Republic of Korea; taekyeong.jin@mail.hongik.ac.kr (T.J.); jjm0511@mail.hongik.ac.kr (J.C.); dyjang1224@mail.hongik.ac.kr (D.J.)
* Correspondence: hschoo@hongik.ac.kr

Abstract: This paper presents a method for predicting atmospheric duct conditions from a clutter power spectrum using deep learning. To accurately predict the duct conditions, deep learning with a binary classification is applied to the proposed refractivity from the clutter (RFC) method. The input data set is the artificial clutter data that are generated via the Advanced Refractive Prediction System (AREPS) simulation software Ver. 3.6 in conjunction with random atmospheric refractive indices. The output of the RFC method is then predicted via binary classification, indicating whether the atmospheric conditions are duct or non-duct. For the cross-validation, the clutter power spectrum data are generated based on real atmospheric refractivity data. The results show that the DNN trained with 5600 pieces of data (validation accuracy of 95.99%) exhibits a binary classification accuracy of 98.36%. The deep neural network (DNN) trained with 28,000 pieces of data (validation accuracy of 98.20%) achieves a binary classification accuracy of 99.06% with an F1-score of 0.9921.

Keywords: radio propagation; radar; deep learning; RFC; binary classification; clutter power

Citation: Jin, T.; Cho, J.; Jang, D.; Choo, H. Prediction of Atmospheric Duct Conditions from a Clutter Power Spectrum Using Deep Learning. *Remote Sens.* **2024**, *16*, 674. https://doi.org/10.3390/rs16040674

Academic Editor: Joan Bech

Received: 28 November 2023
Revised: 24 January 2024
Accepted: 11 February 2024
Published: 14 February 2024

1. Introduction

In long-range radar applications, detecting targets earlier at a longer distance has been a primary concern, and extensive research has been conducted to achieve this ultimate goal [1–6]. This is because the detection accuracy of long-range radar systems often degrades due to the atmospheric refractivity since the electromagnetic waves emitted from radars propagate along a bent path rather than a straight path. With regard to the atmospheric refractivity, atmospheric conditions are classified as normal, super, sub, and duct [7–10]. Among these, the duct conditions have been reported to cause a fatal degradation in the detection performance in the case of long-range targets because such conditions increase the gradient of the atmospheric refractivity index above a certain threshold, making it similar to a waveguide [11,12]. Therefore, it is important to monitor the duct conditions in real time by measuring atmospheric refractivity in terms of the altitude. However, these measurements are typically performed only twice a day at a limited number of meteorological observatories using a radiosonde [13–15]. To resolve such problems, a method estimating refractivity from clutter (RFC) has been proposed [16,17], which derives the atmospheric refractivity index by utilizing radar sea-clutter images in conjunction with various estimation techniques, such as the Kalman filter, the particle filter, and the Bayesian approach [18,19]. Recently, attempts have been made to apply optimization algorithms, such as the genetic algorithm (GA), particle swarm, and simulated annealing (SA), to the RFC techniques [20–22], which allow the duct conditions to be more accurately predicted through the observed clutter power spectrum. However, these methods using the optimization algorithms have a significant drawback of requiring a considerable calculation time to derive a solution, making it difficult to apply for actual radar systems that need real-time calibration. In this context, deep learning methods can be an attractive solution for the creation of an RFC that can be applied to real-time radar systems, and in fact, few

studies of the prediction of atmospheric conditions using deep learning methods have recently been reported [23–26].

In this paper, we propose a method for estimating duct conditions in real time from the clutter power spectrum using deep learning techniques. To accurately estimate the duct condition, the deep learning with the binary classification is applied to the proposed RFC method. In radar operations, clutter power acts in the same way as noise, often degrading target detection performance. In other words, radar performance generally improves as the clutter power decreases. However, since the clutter power fluctuates in real time according to the various atmospheric conditions, it can also be used as an efficient tool to predict the presence of ducts in the direction toward which the radar is oriented. This clutter power can not only be obtained by conducting actual measurements but also be artificially generated using theoretical approaches. In this study, the input data set for the proposed RFC method is the artificial clutter data generated via the Advanced Refractive Prediction System (AREPS) simulation software Ver. 3.6 [27] in conjunction with random atmospheric refractive indices. A simple bi-linear model is employed to generate as many random atmospheric refractive indices as possible, where the slope and thickness of the model are randomly varied through Monte Carlo simulations. Since this model can simply and quickly generate a large amount of learning data, the estimation accuracy of the proposed method can be improved. The output of the RFC method is then predicted, with the binary classification indicating whether the atmospheric conditions are duct or non-duct. In particular, for the training and validation of the RFC method, the input of the artificial clutter data requires labeling to indicate whether the atmospheric conditions are the duct or non-duct. In order to label the duct properly, the average clutter power spectrum is calculated, and then labeling is carried out based on the specific threshold, considering the actual radar system. Subsequently, the proposed deep neural network (DNN) system, consisting of four hidden layers, is trained and validated using 28,000 samples of artificial clutter data, from which the proposed RFC model is able to achieve a validation accuracy of over 98%. Finally, the performance of the RFC model is cross-validated using more realistic clutter power spectrum data, which are generated based on real atmospheric refractivity data obtained from the Heuksando meteorological observatory between 2016 and 2022. In this process, customized hyperparameters that can improve the estimation accuracy are applied to the proposed DNN model. The resulting estimation accuracy is over 99%, confirming that the proposed RFC method can be applied to a real-time radar system to evaluate the presence of a duct within a short time.

2. Calculation of Clutter Power Spectrums

Figure 1 illustrates the proposed RFC method, which used deep learning techniques to predict the duct conditions in real time during the operation of shipborne radar systems. As shown in Figure 1a, electromagnetic waves emitted from the radar were affected by various atmospheric conditions, which could be classified based on the gradient of the modified refractive index in terms of altitude. The modified refractive index M could be calculated using the following equation [28]:

$$N = \left(77.6 \times \frac{P}{T} + 72 \times \frac{e}{T} + 3.75 \times 10^5 \times \frac{e}{T^2}\right) \quad (1)$$

$$M(h) = N(h) + 157 \times h \quad (2)$$

where P and e are the atmospheric pressure and the pressure of the water vapor, respectively. T means the absolute temperature in K, and N is the radio refractivity, which can be calculated using P, e, and T. The refractivity index M was used instead of N to compensate for the Earth's curvature for altitude h. Herein, the standard atmospheric condition occurred when the gradient of the modified refractivity (∇M) was 117, and it was called the normal atmospheric condition when ∇M was in the range of $78 \leq \nabla M \leq 157$. If $\nabla M > 157$, it was in a sub-atmospheric condition, while if $0 \leq \nabla M < 78$, it was in a super-atmospheric condition.

In particular, a ∇M less than 0 meant a duct condition, which could significantly affect the propagation path of the electromagnetic waves. Thus, it was important to predict the duct conditions in real time. Such predictions can be used in various fields, such as radar systems, military operations, aviation safety, and wireless communications [29–33]. In the duct condition, electromagnetic waves from a radar were trapped along the Earth's surface, which resulted in the radar receiving strong clutter power from the sea surface or terrain. Therefore, the occurrence of a duct could be assumed when a stronger-than-usual clutter power spectrum was observed. The proposed RFC method for predicting duct conditions could be summarized in a three-step procedure, as shown in Figure 1b. Firstly, clutter power spectrums, which could be artificially created or obtained from real radar, were generated. Following this step, the clutter power spectrum was used as the input for the proposed RFC method. The output of the RFC method was then a classification indicating whether the condition was duct or non-duct for the input clutter power spectrum. Secondly, the artificially created clutter power spectra (amounting to 28,000), labeled according to the presence of ducts, were used to train and validate the DNN consisting of four hidden layers. Finally, the proposed RFC method was cross-validated using more realistic clutter power spectrum data generated based on real atmospheric refractivity data obtained from the Heuksando meteorological observatory between 2016 and 2022.

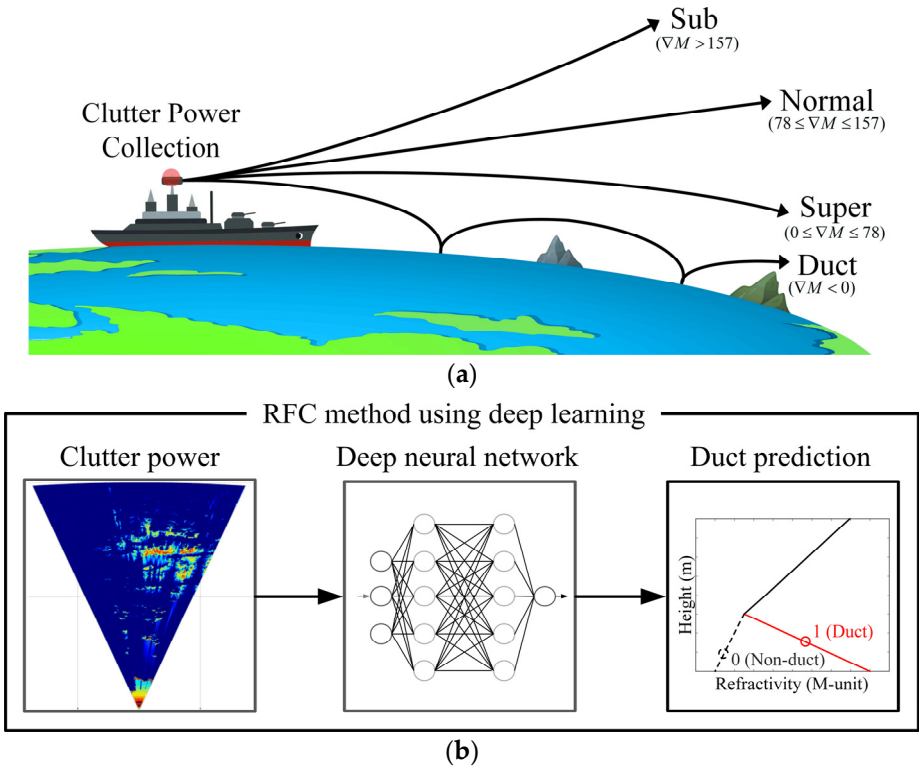

Figure 1. RFC techniques of the shipborne radar using deep learning: (**a**) propagation of electromagnetic waves according to various atmospheric conditions; (**b**) RFC method using deep learning.

Figure 2 presents the bi-linear model employed in the proposed RFC method to derive the various atmospheric refractive indices to obtain artificial clutter power spectrums. A bi-linear model was employed for this purpose because it offered the simplest representation of the four aforementioned atmospheric conditions. Such a model could be perceived as dealing with two regions determined via two specific linear functions, expressed as follows [34]:

$$M(h) = M(0) + \begin{cases} d_1 h & h < h_1 \\ d_2(h - h_1) + d_1 h_1 & h \geq h_1 \end{cases} \quad (3)$$

where $M(0)$ is the modified refractivity at altitude 0 m, typically taken as 330 M-unit [34], and h is the height from the sea surface. h_1 indicates the height of the boundary dividing the two regions. d_1 and d_2 denote the slopes of the line in the bottom and top regions, respectively. This study primarily focused on predicting the refractive index in low-altitude regions, since the propagation path of electromagnetic waves emanating from a shipborne radar was mainly affected by the refractive index of the atmosphere close to the sea surface. The height h_1 and slope d_1 represent the regions closest to the sea surface, which were also the important variables for the bi-linear model. The slope d_2 denotes the high-altitude region, which was fixed at a standard atmospheric value of 117 M-unit/m in this study. In the bi-linear model, h_1 and d_1 were randomly generated, characterized by a uniform distribution ranging from 0 m to 300 m and −300 M-unit/m to 300 M-unit/m, respectively.

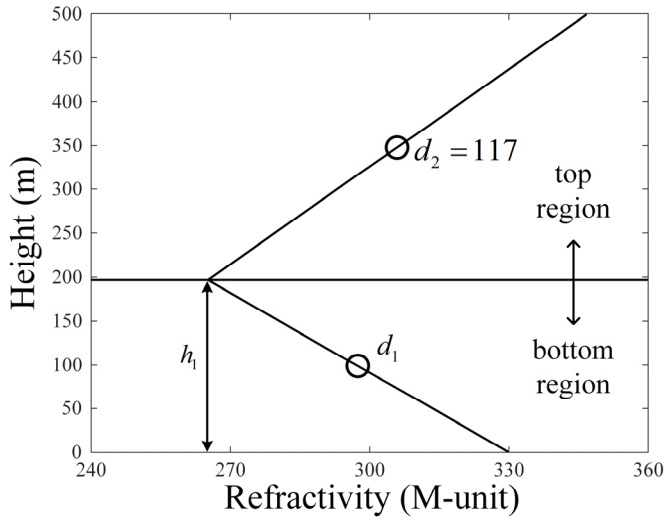

Figure 2. Bi-linear model representing various atmospheric conditions.

Figure 3 shows the path loss for two cases with different atmospheric refractive indices. One of them is a surface duct case (h_1 = 300 m, d_1 = −200 M-unit/m), while the other is a normal case (h_1 = 300 m, d_1 = 117 M-unit/m). The path loss for each cases was obtained using the AREPS EM propagation simulator, with the atmospheric refractive indices used as the input data for this simulator. The radar system considered here was an L-band ship radar system with a high radiating power of 1.95 MW that could detect targets located up to 360 km away [35]. The mounted height of the radar was 30 m, and its operating frequency was 1.3 GHz. We then observed the path loss levels at a distance of 100 km near the surface (altitude of 50 m). In Figure 3a, in the case of a surface duct condition, radar wave propagation was trapped along the sea surface, resulting in a low path loss of 128.8 dB at the observation point. In contrast, under normal conditions, the trapped wave moving along the sea surface could not be observed, as shown in Figure 3b, resulting in a higher path loss of 179.8 dB at the observation point.

Figure 4 represents the clutter power spectrum for the two cases with different atmospheric refractive indices, as calculated from the path loss using the following equation [36]:

$$P_c = \frac{P_t G^2 \lambda^2 \sigma}{L 4\pi r^2} \tag{4}$$

$$L = \frac{(4\pi r)^2}{\lambda^2} \tag{5}$$

$$\sigma = A\sigma_0 \tag{6}$$

where P_t and G are the transmitted power and the radar antenna gain, respectively. λ is the wavelength, and L is the path loss in the free space. r is the distance from the

radar [34], and A is the illumination surface area of the electromagnetic wave emitted from the radar. In addition, σ_0 represents the normalized radar cross-section of the sea surface [37]. Under normal conditions, the average of the clutter power spectrums was observed to be −344.5 dBm. In contrast, a strong average clutter power of −81.3 dBm was observed in the case of the duct atmospheric condition.

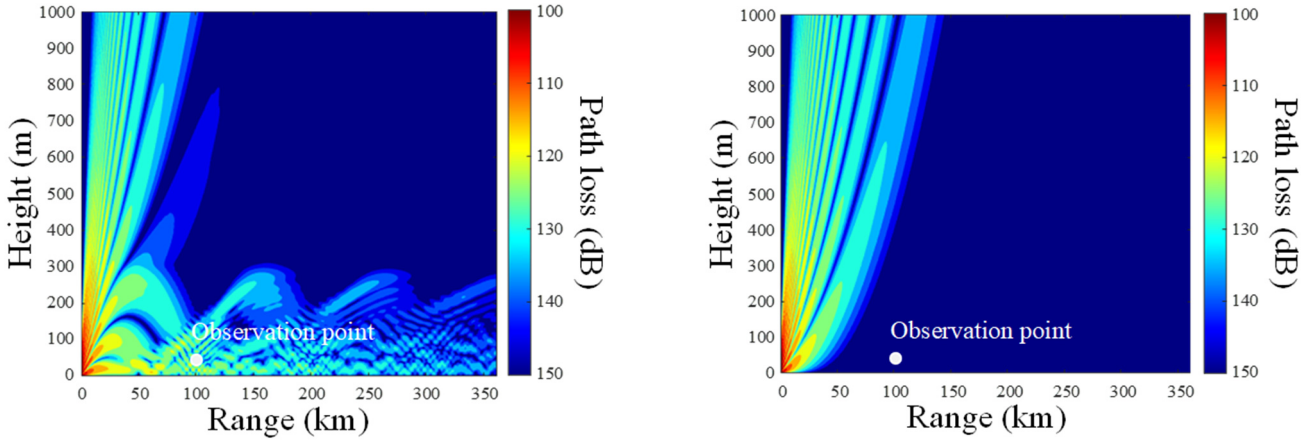

Figure 3. Path loss according to atmospheric conditions: (**a**) duct; (**b**) standard.

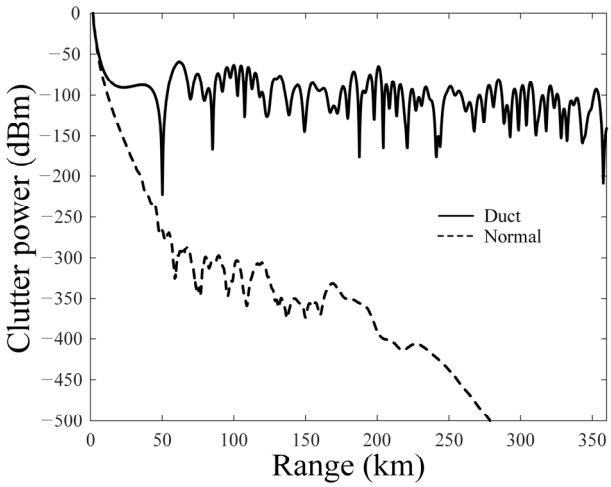

Figure 4. Clutter power spectrum according to the atmospheric conditions.

3. Estimation of an Atmospheric Refractivity Using Deep Learning

Figure 5 presents a detailed flow chart of the proposed RFC method using deep learning techniques. To create the clutter power spectrum data set, the arbitrary bi-linear model was first constructed through the Monte Carlo simulation (with d_1 and h_1 having uniform distributions). The path loss according to the bi-linear model was calculated using the AREPS simulator, and then the clutter power spectrums (amounting to 28,000) were derived, as explained in Figure 4. After obtaining the clutter spectrum data set, each piece of data was labeled to indicate whether the clutter spectrum was caused by duct or non-duct conditions. We examined d_1 and h_1 via the bi-linear model, which resulted in an average clutter spectrum greater than −115 dBm. This study used the specific threshold of −115 dBm since it was the minimum sensitivity at which the radar system can recognize signals above the noise level [35]. Therefore, samples from the clutter spectrum data set with an average greater than −115 dBm were labeled duct (DNN output value of 1), while all other clutter spectrums were labeled non-duct (DNN output value of 0). The labeled

clutter power spectrums were then utilized as inputs for the four-layer DNN to train and validate it. A total of 28,000 pieces of data were used in this process. Finally, the trained DNN took the clutter power spectrum without labels as an input to produce a binary classification output of either 1 or 0, indicating whether it represented duct or non-duct conditions, respectively.

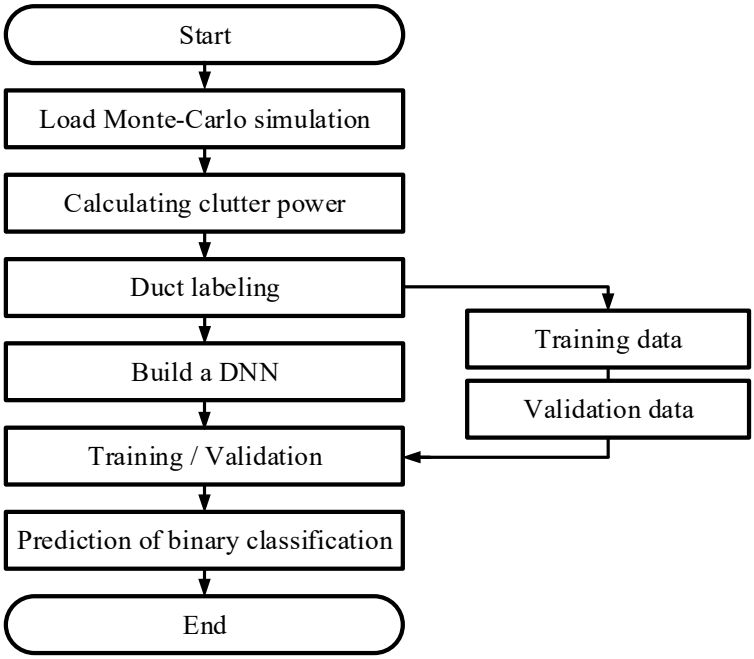

Figure 5. Deep learning process for estimating atmospheric refractivity.

Figure 6 illustrates a map of the average clutter power according to duct slope d_1 and duct thickness h_1. These results can help to identify the conditions for d_1 and h_1 that produce the clutter power with an average greater than −115 dBm. As we mentioned in Chapter 2, atmospheric duct conditions are defined when the value of d_1 is negative. However, a negative d_1 may not generate strong clutter power that significantly degrades the detection performance of the actual radar. Therefore, the conditions of d_1 and h_1 that could cause critical issues for real radar systems were investigated. These criteria were −115 dBm considering the sensitivity of the actual radar systems [35]. The dashed black line in Figure 6 indicates the boundary, where the average clutter power is −115 dBm. Based on the position of this dashed black line, the upper left area represents the duct condition where strong clutter (labeled '1') is generated, while the remaining area indicates the non-duct condition that does not generate significant clutter (labeled '0'). Furthermore, considering the entire data set, the ratio of labels '1' and '0' is found to be 28:72.

Figure 7 provides examples of the four types of atmospheric refractivity collected from the Heuksando meteorological observatory between 2016 and 2022. The Heuksando meteorological observatory is one of seven observatories in the Republic of Korea. The data are provided at 100-meter intervals, resulting in a total of 4902 pieces of data. The measurement data are utilized to evaluate the performance of the proposed RFC method, trained using the artificially constructed bi-linear model. This work was carried out to evaluate the performance of the proposed RFC method using more realistic clutter power data. Similar to the previous estimations, the AREPS simulation software Ver. 3.6 was employed to calculate the clutter power spectrum data obtained from the Heuksando meteorological observatory to generate the clutter power spectrum, which was then used for cross-validation of the trained DNN.

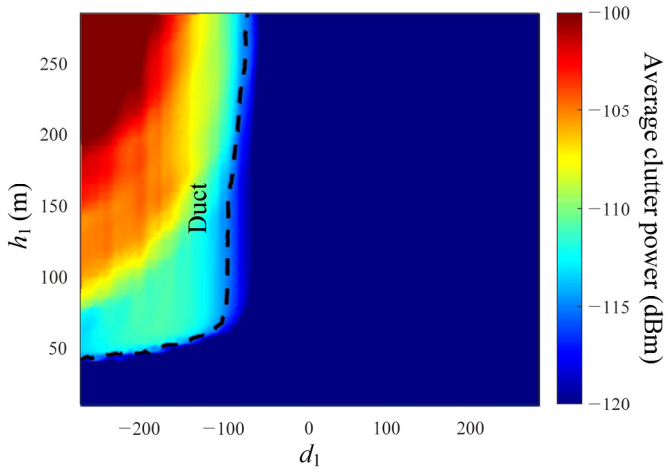

Figure 6. Clutter power map considering d_1 and h_1 in the bi-linear model.

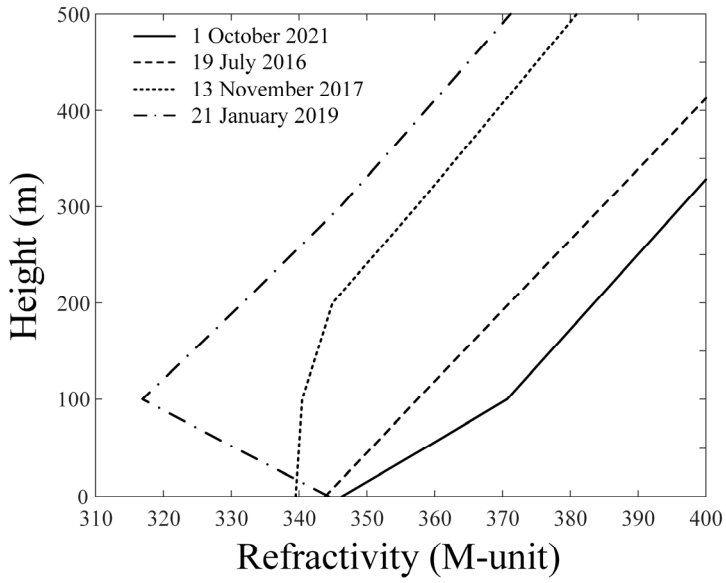

Figure 7. Four examples of atmospheric refractivities collected from the Heuksando meteorological observatory from 2016 to 2022.

Table 1 shows the hyperparameters and number of neurons used in the DNN architecture. The epochs, a minibatch size, a learning rate, and an optimizer are set to 30, 128, 0.01, and Adam [38], respectively. The proposed DNN model consists of four layers, and each layer is connected by a ReLU (Rectified Linear Unit) function. After layer 4, a softmax function is connected to classify the atmospheric conditions, and the loss function is cross-entropy [39]. The numbers of neurons used in the layers (Layer 1, . . ., 4) are 128, 64, 32, and 8, respectively. The clutter power spectrums, labeled based on the presence of a duct, are employed for the training and validation of the DNN.

Table 1. Hyperparameters, number of neurons, and functions used in the DNN architecture.

Hyperparameter		Number of Neurons		Functions	
Epochs	30	Layer 1	128	Activation	ReLU
Minibatch size	128	Layer 2	64	Last classification loss	Softmax
Learning rate	0.01	Layer 3	32		
Optimizer	Adam	Layer 4	8		Cross-entropy

Table 2 represents a summary of the estimation results obtained using deep learning. The prepared data set for the DNN training comprises 28,000 pieces of data, with the ratio of the training data to the validation data being 5:2. Under the conditions outlined in Table 1, the training process takes approximately 70 s to complete, after which the output for a single piece of input data is generated within milliseconds. The results presented in Table 2 show that a minimum of 5600 pieces of data are required to achieve a validation accuracy of over 95% (for both duct and non-duct classification). To attain a validation accuracy of over 98%, a minimum of 28,000 pieces of data are needed. In addition, further estimations are conducted using actual observation data from the Heuksando observatory. The results show that the DNN trained with 5600 pieces of data (validation accuracy of 95.99%) exhibits a binary classification accuracy of 98.36%. The DNN trained with 28,000 pieces of data (validation accuracy of 98.20%) achieves a binary classification accuracy of 99.06%, with an F1-score of 0.9921.

Table 2. Summary of the estimation results obtained using deep learning.

Total Number of Data Items	Validation Accuracy	Prediction Accuracy with the Heuksando Data
2800	94.35%	98.31%
5600	95.99%	98.36%
8400	96.63%	98.53%
11,200	97.43%	98.43%
14,000	97.77%	98.84%
28,000	98.20%	99.06%

Table 3 shows the comparisons with previous studies using DNN models for the RFC. In Ref. [24], the slope and thickness of the ducts are estimated using the DNN model from the sea clutter spectrum, but this study only used a small amount of training data, less than 3000 samples. Refs. [25,26] used a large amount of data, more than 30,000 samples, but cross-validation with the real data was not performed. On the other hand, our study performed cross-validation using real atmospheric data. In addition, the proposed method achieved a prediction accuracy of over 99% with a short estimation time of 160 milliseconds. Furthermore, compared to the traditional methods for the RFC, such as the GA [20], Kalman Filter [40], and look-up table matching [41], the proposed estimation method has the advantages of being able to predict various atmospheric conditions in a short time while using a relatively small number of preparation data items.

Table 3. Comparisons with previous studies using DNN models.

	Proposed Method	[24]	[25]	[26]
Training data set (max.)	28,000	3000	100,000	35,000
The number of layers	4	4	5	6
Total number of neurons	232	No specified	475	3000
Cross-validation data	Real refractivity data	-	-	-

4. Conclusions

We investigated the method for predicting atmospheric duct conditions from the clutter power spectrum using deep learning. The input data set for the proposed RFC method was the artificial clutter data, generated using the AREPS simulation software Ver. 3.6 in conjunction with random atmospheric refractive indices. The output of the RFC method was then predicted via binary classification, indicating whether the atmospheric conditions were duct or non-duct. The prepared data set for DNN training comprised 28,000 pieces of data, with the ratio of the training data to the validation data being 5:2. The results showed that the proposed RFC methods required a minimum of 5600 pieces of data to reach a validation accuracy of over 95%. A minimum of 28,000 data were needed to reach a validation accuracy of over 98%. Furthermore, when using actual

observation data from Heuksando, the DNN with 5600 pieces of data exhibited a binary classification accuracy of 98.36%. The DNN with 28,000 pieces of data showed a binary classification accuracy of 99.06%. These results demonstrated that the proposed RFC method is suitable for application in real-time radar systems responsible for evaluating the presence of a duct within a short time. The proposed method focused on classifying the duct condition; thus, this method is not suitable for estimating the other atmospheric conditions. Therefore, our future work will aim to predict all atmospheric conditions using a multi-class classification method.

Author Contributions: Conceptualization, T.J., J.C., D.J. and H.C.; methodology, T.J.; software, T.J., J.C. and D.J.; validation, T.J., J.C., D.J. and H.C.; formal analysis, T.J.; investigation, J.C.; resources, T.J.; data curation, T.J.; writing—original draft preparation, T.J.; writing—review and editing, T.J., J.C., D.J. and H.C.; visualization, T.J.; supervision, H.C.; project administration, H.C.; funding acquisition, H.C. All authors have read and agreed to the published version of the manuscript.

Funding: This research received no external funding.

Data Availability Statement: Data are contained within the article.

Acknowledgments: This work was supported by the Basic Science Research Program through the National Research Foundation of Korea (NRF), funded by the Ministry of Education (No. NRF-2017R1A5A1015596), and the NRF grant, funded by the Korean Government (No. 2015R1A6A1A03031833; NRF-2017R1D1A1B04031890).

Conflicts of Interest: The authors declare no conflicts of interest.

References

1. Raja Abdullah, R.S.A.; Salah, A.A.; Ismail, A.; Hashim, F.H.; Rashid, N.E.A.; Aziz, N.H.A. Experimental investigation on target detection and tracking in passive radar using long-term evolution signal. *IET Radar Sonar Navig.* **2016**, *10*, 577–585. [CrossRef]
2. Locker, C.; Vaupel, T.; Eibert, T.F. Radiation efficient unidirectional low-profile slot antenna elements for X-band application. *IEEE Trans. Antennas Propag.* **2005**, *53*, 2765–2768. [CrossRef]
3. Dastkhosh, A.R.; Oskouei, H.D.; Khademevatan, G. Compact low weight high gain broadband antenna by polarization-rotation technique for X-band radar. *Int. J. Antennas Propag.* **2014**, *2014*, 743046. [CrossRef]
4. Zhou, Y.; Wang, T.; Hu, R.; Su, H.; Liu, Y.; Liu, X.; Suo, J.; Snoussi, H. Multiple kernelized correlation filters (MKCF) for extended object tracking using X-band marine radar data. *IEEE Trans. Signal Process.* **2019**, *67*, 3676–3688. [CrossRef]
5. Wang, A.; Krishnamurthy, V. Signal interpretation of multifunction radars: Modeling and statistical signal processing with Stochastic Context Free Grammar. *IEEE Trans. Signal Process.* **2008**, *56*, 1106–1119. [CrossRef]
6. Wang, S.; Jang, D.; Kim, Y.; Choo, H. Design of S/X-Band dual-loop shared-aperture 2 × 2 array antenna. *J. Electromagn. Eng. Sci.* **2022**, *22*, 319–325. [CrossRef]
7. Lim, T.H.; Go, M.; Seo, C.; Choo, H. Analysis of the target detection performance of Air-to-Air airborne radar using long-range propagation simulation in abnormal atmospheric conditions. *Appl. Sci.* **2020**, *10*, 6440. [CrossRef]
8. Lim, T.; Choo, H. Prediction of target detection probability based on air-to-air long-range scenarios in anomalous atmospheric environments. *Remote Sens.* **2021**, *13*, 3943. [CrossRef]
9. Sharma, V.; Kumar, L. Photonic-radar based multiple-target tracking under complex traffic-environments. *IEEE Access* **2020**, *8*, 225845. [CrossRef]
10. Kim, I.; Kim, H.; Lee, J.-H. Theoretical minimum detection range for a rapidly moving target and an experimental evaluation. *J. Electromagn. Eng. Sci.* **2021**, *21*, 161–164. [CrossRef]
11. Reilly, J.P.; Dockery, G.D. Influence of evaporation ducts on radar sea return. *IEE Proc. F (Radar Signal Process.)* **1990**, *137*, 80–88. [CrossRef]
12. Huang, L.F.; Liu, C.G.; Wang, H.G.; Zhu, Q.L.; Zhang, L.J.; Han, J.; Zhang, Y.S.; Wang, Q.N. Experimental analysis of atmospheric ducts and navigation radar over-the-horizon detection. *Remote Sens.* **2022**, *14*, 2588. [CrossRef]
13. Tedesco, M.; Wang, J.R. Atmospheric correction of AMSR-E brightness temperatures for dry snow cover mapping. *IEEE Geosci. Remote Sens. Lett.* **2006**, *3*, 320–324. [CrossRef]
14. Wang, J.R.; Racette, P.; Triesky, M.E.; Browell, E.V.; Ismail, S.; Chang, L.A. Profiling of atmospheric water vapor with MIR and LASE. *IEEE Geosci. Remote Sens. Lett.* **2002**, *40*, 1211–1219. [CrossRef]
15. Birkemeier, W.P.; Duvosin, P.F.; Fontaine, A.B.; Thomson, D.W. Indirect atmospheric measurements utilizing rake tropospheric scatter techniques—Part II: Radiometeorological interpretation of rake channel-sounding observations. *Proc. IEEE* **1969**, *57*, 552–559. [CrossRef]
16. Douvenot, R.; Fabbro, V. On the knowledge of radar coverage at sea using real time refractivity from clutter. *IET Radar Sonar Navig.* **2010**, *4*, 293–301. [CrossRef]

17. Douvenot, R.; Fabbro, V.; Gerstoft, P.; Bourlier, C.; Saillard, J. Real time refractivity from clutter using a best fit approach improved with physical information. *Radio Sci.* **2010**, *45*, 1–13. [CrossRef]
18. Yardim, C.; Gerstoft, P.; Hodgkiss, W.S. Tracking refractivity from clutter using Kalman and Particle filters. *IEEE Trans. Antennas Propag.* **2008**, *56*, 1058–1070. [CrossRef]
19. Yardim, C.; Gerstoft, P.; Hodgkiss, W.S. Estimation of radio refractivity from radar clutter using Bayesian Monte Carlo analysis. *IEEE Trans. Antennas Propag.* **2006**, *54*, 1318–1327. [CrossRef]
20. Jang, D.; Kim, J.; Park, Y.B.; Choo, H. Study of an Atmospheric Refractivity Estimation from a Clutter Using Genetic Algorithm. *Appl. Sci.* **2022**, *12*, 8566. [CrossRef]
21. Wang, B.; Wu, Z.S.; Zhao, Z.; Wang, H.G. Retrieving evaporation duct heights from radar sea clutter using particle swarm optimization (PSO) algorithm. *Progress Electromagn. Res. M* **2009**, *9*, 79–91. [CrossRef]
22. Huang, S.-X.; Zhao, X.-F.; Sheng, Z. Refractivity estimation from radar sea clutter. *Chin. Phys. B* **2009**, *18*, 5084–5090.
23. Ji, H.; Yin, B.; Zhang, J.; Zhang, Y. Joint inversion of evaporation duct based on radar sea clutter and target echo using deep learning. *Electronics* **2022**, *11*, 2157. [CrossRef]
24. Guo, X.; Wu, J.; Zhang, J.; Han, J. Deep learning for solving inversion problem of atmospheric refractivity estimation. *Sustain. Cities Soc.* **2018**, *43*, 524–531. [CrossRef]
25. Tang, W.; Cha, H.; Wei, M.; Tian, B.; Ren, X. An atmospheric refractivity inversion method based on deep learning. *Results Phys.* **2019**, *12*, 582–584. [CrossRef]
26. Cui, M.Y.; Zhang, Y. Deep Learning Method for Evaporation Duct Inversion Based on GPS Signal. *Atmosphere* **2022**, *13*, 2091. [CrossRef]
27. *Advanced Refractive Prediction System (AREPS)*; Ver. 3.6; The Space and Naval Warfare System: San Diego, CA, USA, 2005.
28. ITU. The Radio Refractive Index: Its Formula and Refractivity Data. ITU-R P.453. 2019. Available online: https://www.itu.int/rec/R-REC-P.453/en (accessed on 8 September 2019).
29. Liu, F.; Pan, J.; Zhou, X.; Li, G.Y. Atmospheric ducting effect in wireless communications: Challenges and opportunities. *J. Commun. Inf. Netw.* **2021**, *6*, 101–109. [CrossRef]
30. Yang, C.; Wang, J. The investigation of cooperation diversity for communication exploiting evaporation ducts in the south China Sea. *IEEE Trans. Antennas Propag.* **2022**, *70*, 8337–8347. [CrossRef]
31. Zhang, H.; Zhou, T.; Xu, T.; Wang, Y.; Hu, H. Statistical modeling of evaporation duct channel for maritime broadband communications. *IEEE Trans. Veh. Technol.* **2022**, *71*, 10228–10240. [CrossRef]
32. Ma, J.; Wang, J.; Yang, C. Long-range microwave links guided by evaporation ducts. *IEEE Commun. Mag.* **2022**, *60*, 68–72. [CrossRef]
33. Lim, T.H.; Wang, S.; Chong, Y.J.; Park, Y.B.; Ko, J.; Choo, H. High altitude ducts causing abnormal wave propagation in coastal area of Korea. *Microw. Opt. Technol. Lett.* **2020**, *62*, 643–650. [CrossRef]
34. Yang, C.; Wang, Y.; Zhang, A.; Fan, H.; Guo, L. A Random Forest Algorithm Combined with Bayesian Optimization for Atmospheric Duct Estimation. *Remote Sens.* **2023**, *15*, 4296. [CrossRef]
35. Sanders, F.H.; Sole, R.L.; Bedford, B.L.; Franc, D.; Pawlowitz, T. *Effects of RF Interference on Radar Receiver*; Institute for Telecommunication Sciences: Boulder, CO, USA, 2006.
36. Compaleo, J.; Yardim, C.; Xu, L. Refractivity-from-clutter capable, software-defined, coherent-on-receive marine radar. *Radio Sci.* **2021**, *56*, 1–19. [CrossRef]
37. Nathanson, F.E.; Reilly, J.P.; Cohen, M. *Radar Design Principles*, 2nd ed.; McGraw-Hill: New York, NY, USA, 1991.
38. Hassan, E.; Shams, M.Y.; Hikal, N.A.; Elmougy, S. The effect of choosing optimizer algorithms to improve computer vision tasks: A comparative study. *Multimedia Tools Appl.* **2023**, *82*, 16591–16633. [CrossRef] [PubMed]
39. Jamin, A.; Humeau-Heurtier, A. (Multiscale) cross-entropy methods: A review. *Entropy* **2019**, *22*, 45. [CrossRef]
40. Do, P.N.; Chung, K.S.; Feng, Y.C.; Lin, P.L.; Tsai, B.A. Assimilation of Radar-Derived Refractivity and Radar Data in the Context of Ensemble Kalman Filter: Cases Study of the Southwest Monsoon Experiment. *Q. J. R. Meteorol. Soc.* **2023**, *149*, 1365–1390. [CrossRef]
41. Skiles, S.M.; Painter, T.; Okin, G.S. A method to retrieve the spectral complex refractive index and single scattering optical properties of dust deposited in mountain snow. *J. Glaciol.* **2017**, *6*, 133–147. [CrossRef]